

Experimental Tests of Quasisymmetry in HSX

J.N. TALMADGE, F.S.B. ANDERSON, D.T. ANDERSON, C. DENG¹), W. GUTTENFELDER, K.M. LIKIN, J. LORE, J.C. SCHMITT and K. ZHAI

HSX Plasma Laboratory, University of Wisconsin-Madison, USA

¹*University of California-Los Angeles, USA*

(Received 27 November 2007 / Accepted 7 March 2008)

This paper discusses the results from experiments in HSX testing the properties of a quasisymmetric stellarator. HSX is a quasihelical stellarator with minimal toroidal curvature and a high effective transform. The high effective transform was verified from passing particle orbits as well as from the magnitude of the Pfirsch-Schlüter and bootstrap currents. The passing particle orbit shift, the helical structure of the Pfirsch-Schlüter current and the direction of the bootstrap current were all consistent with the lack of toroidal curvature. Good agreement was observed between data from plasma currents obtained by a set of magnetic pick-up coils and the results of the V3FIT code. Good confinement of trapped particles was observed with quasisymmetry. These particles may be responsible for a coherent global MHD mode that was detected during ECH at $B = 0.5$ T. It was found that the breaking of quasisymmetry increased the hollowness of the density profile and the damping of plasma flow while decreasing the core electron temperature, in good agreement with neoclassical models. At 0.5 T, anomalous transport appeared unaffected by the degree of quasisymmetry; more work is needed to understand if this still holds at 1.0 T. The experimental energy confinement time and electron temperature profile could be reproduced reasonably well with a combination of neoclassical transport and a modified Weiland model for ITG/TEM turbulence.

© 2008 The Japan Society of Plasma Science and Nuclear Fusion Research

Keywords: quasisymmetry, HSX, quasihelical symmetry, transport, effective transform, bootstrap current, Pfirsch-Schlüter current, turbulence

DOI: 10.1585/pfr.3.S1002

1. Introduction

The poor neoclassical transport in the low collisionality regime of conventional stellarators has spurred efforts to design stellarators which combine the good single particle confinement of the tokamak and the steady-state, disruption-free characteristics of stellarators. The paper by Mynick [1] summarizes various approaches by which neoclassical transport in stellarators might be improved. One such approach is the quasisymmetric stellarator, pioneered by Nührenberg and Zille [2] and by Garabedian [3]. A quasisymmetric stellarator is one in which the magnetic field spectrum is dominated by a single harmonic. Aside from the tokamak-like neoclassical transport, quasisymmetric stellarators possess a direction of symmetry in $|B|$ and hence minimal parallel viscous damping in that direction. Such a property may be advantageous for improving anomalous transport by reducing the damping of zonal flow [4, 5].

The quasisymmetric approach to improving transport in stellarators is the thrust of the U.S. stellarator program. The Helically Symmetric Experiment (HSX) [6] is the first quasisymmetric stellarator in the world. The symmetry in this experiment is in the helical direction. The quasi-axisymmetric National Compact Stellarator Experiment (NCSX) [7], is symmetric in the toroidal direction

author's e-mail: talmadge@wisc.edu

and is currently under construction at PPPL. Finally, the proposed Quasi Poloidal Stellarator (QPS) [8] at ORNL has a direction of symmetry in the poloidal direction.

In Boozer coordinates, the magnitude of the magnetic field for a quasihelically symmetric (QHS) stellarator can be written as

$$B/B_0 = 1 - b_{nm} \cos(n\phi - m\theta), \quad (1)$$

where ϕ is the toroidal angle and θ is the poloidal angle. In a straight field-line coordinate system given by $\theta = \epsilon\phi$, where ϵ is the rotational transform, the magnetic field variation on the field line is given by

$$B/B_0 = 1 - b_{nm} \cos([n - m\epsilon]\phi). \quad (2)$$

This is similar to the variation along a field line in a tokamak with the substitution $\epsilon_{\text{eff}} = n - m\epsilon$ for the rotational transform. For HSX, with $n = 4$, $m = 1$ and $\epsilon \geq 1$, the effective transform ϵ_{eff} is about 3.

The combination of quasisymmetry and high effective transform in HSX results in small drifts of passing particles from a flux surface, small banana widths, small plasma currents, low neoclassical transport and low parallel viscous damping. On the other hand, the high curvature and small connection length in HSX may be responsible for somewhat larger anomalous transport. This paper dis-

cusses what recent experimental results from HSX can tell us about the properties of a quasisymmetric stellarator.

2. Drift Orbits

The leading $m \neq 0$ terms of the vacuum magnetic field spectrum in HSX were determined by measuring the orbit shift of passing electrons from a flux surface [9]. At low energies, the electrons injected with a filament stay close to the flux surface and were used to map the lab coordinate frame into Boozer coordinates using a neural network. At higher energies, the electrons deviate from the flux surface and measurement of this deviation at several toroidal locations yields the spectrum.

The direction of the shift of the electron from a magnetic surface is a verification of the lack of toroidal curvature in HSX. Figure 1 is a comparison of the contours

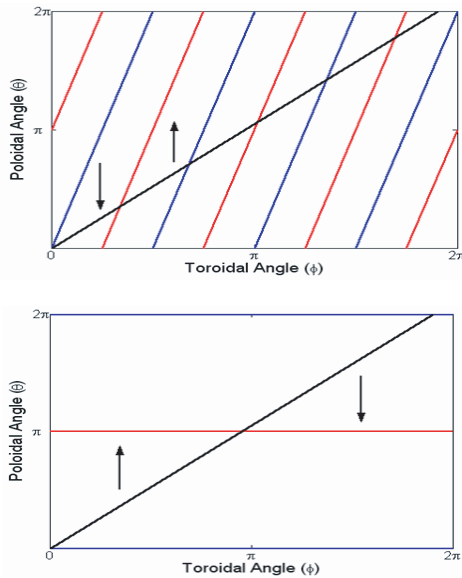


Fig. 1 Contours of constant $|B|$ for a quasisymmetric configuration (top) and for a tokamak (bottom). Also shown is a magnetic field line with a rotational transform of 1.06. The arrows point in the direction of increasing $|B|$ in the poloidal direction. Red is the maximum field, blue is the minimum.

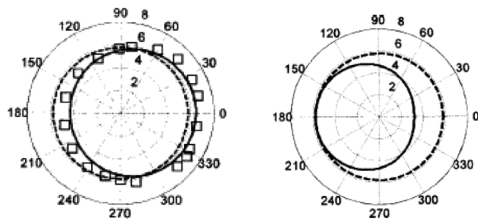


Fig. 2 Experimental data from HSX mapped into Boozer coordinates (left) and a calculation of the orbit of the same electron in a tokamak magnetic field (right). The dashed line is a flux surface and the solid line is the particle orbit.

of constant $|B|$ in HSX and in a tokamak. Along a magnetic field line close to a toroidal angle of zero degrees, the direction of increasing B is oppositely directed in the two cases. Since the radial drift velocity in Boozer coordinates for a curl-free magnetic field is given by $B_0 r dr/dt = -(mv_{\parallel}^2/eB)dB/d\theta$, the radial drift from the home flux surface should be in the opposite direction for the two configurations. Figure 1 also illustrates the high effective transform that is characteristic of quasihelically symmetric stellarators. For the QHS configuration, as the magnetic field line rotates once around the magnetic axis poloidally, $|B|$ undergoes just under 3 oscillations. For the corresponding tokamak with the same transform, there is 1 oscillation. Another way to look at it is to see that the gradient of $|B|$ changes sign over a much smaller spatial scale in a QHS device than in a tokamak, resulting in smaller deviation from a flux surface.

The plot on the left of Fig. 2 shows the measured electron orbit in HSX after mapping to Boozer coordinates. The deviation of the orbit from a flux surface is due to the $n = 4, m = 1$ helical field on the right side of the experimental data and to the $n = 1, m = 1$ earth's field on the left. The earth's field is significant in this case because the experiment was done at a magnetic field of only 90 gauss; at higher fields the earth's field can be neglected. The plot on the right of Fig. 2 is a calculated orbit of the electron if it were in a tokamak (neglecting the earth's field). Comparing the two figures it can be seen that indeed the orbit shift on the right side of each plot is outside the flux surface for the QHS case and inside the surface for the tokamak. Also, the orbit shift is smaller for the QHS case because of the higher effective transform.

3. Pfirsch-Schlüter and Bootstrap Currents

Because of the lack of toroidal curvature in HSX, the Pfirsch-Schlüter (PS) and bootstrap currents have some unique properties. For a quasihelically symmetric configuration, the PS current is given by Boozer [10],

$$J_{PS} = \frac{1}{B_0} \frac{dp}{d\psi} \frac{nI + mg}{n - m\epsilon} \delta_{nm} \cos(n\phi - m\theta), \quad (3)$$

and the bootstrap current has the expression [11],

$$J_{BS} = 1.46 \sqrt{b_{nm}} \frac{m}{n - m\epsilon} \frac{g}{B_0} \left[1.67(T_e + T_i) \frac{dn}{d\psi} + 0.47n \frac{dT_e}{d\psi} - 0.29n \frac{dT_i}{d\psi} \right]. \quad (4)$$

There are several things to notice about these expressions. For one thing, both currents are reduced by the same factor, $n - m\epsilon$ which is the effective transform. Also, the Pfirsch-Schlüter current is helical so that from the beginning of the field period to the half-period the dipole currents reverse direction. Note that at $\phi = 0^\circ$ where the magnetic field in a QHS device is tokamak-like (that is, the high field side is

on the inboard side), the PS current distribution is reversed from what it would be in a tokamak. From the equation this appears as a sign change between an $n = 4, m = 1$ and an $n = 0, m = 1$ configuration. Physically this effect occurs because of the reversal in the gradient of the magnetic field between a QHS and tokamak configuration, just like in the particle orbit. Note too, that the bootstrap current in a QHS device is in the opposite direction from that in a tokamak, resulting in a rotational transform that decreases as the pressure gradient increases. The transport however doesn't degrade with the decrease in the transform, because the effective transform actually increases slightly.

The reversal of the bootstrap current in a QHS device compared to a tokamak can be understood using the model developed by Shaing and Callen [12]. The top plot of Fig. 3 shows how the parallel current flows in one direction for HSX so that when added to the diamagnetic current, the total current flows along the direction of symmetry. The bottom plot shows how this parallel current has to flow in the opposite direction along the field line so that the total current flows in the toroidal direction.

To measure the plasma current in HSX there is a Rogowski coil and a belt to which is attached a set of 16 3-axis magnetic coils. Both are mounted outside the vacuum chamber of HSX. To measure the signals due to the helical PS current, the belt containing the set of 16 triplets was first placed at the half-field period and subsequently at the one-sixth period location. Figure 4 is an illustration of the helical nature of the current and the approximate locations of the 16 triplets. The red and blue colors denote currents

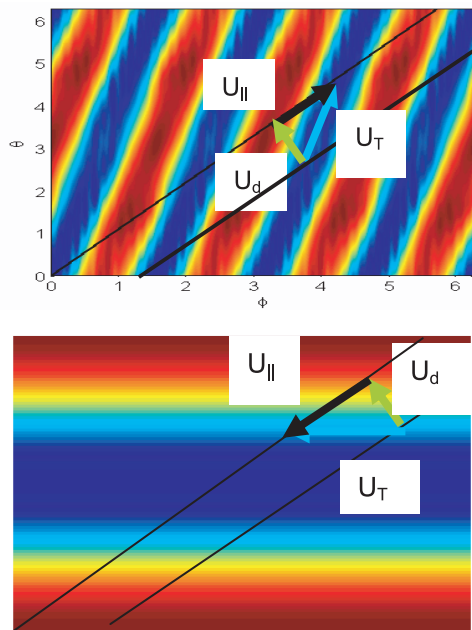


Fig. 3 Diamagnetic current (U_d), parallel bootstrap current ($U_{||}$) and total current (U_T) in HSX (top) and a tokamak (bottom) illustrating how the bootstrap current flows in opposite directions for the two configurations.

that are flowing in the opposite directions.

Figure 5 shows the poloidal and radial magnetic fields due to the plasma current at a time, late in the discharge, just before the ECH is turned off. It can be seen from the figure that the radial magnetic field at the 1/2 field period is almost 180° degrees out of phase with the signals at the 1/6 field period location. This confirms that indeed the PS current in HSX is helical.

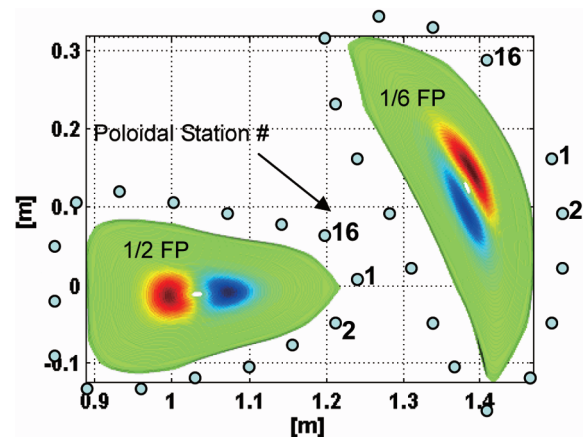


Fig. 4 Last closed magnetic surface and Pfirsch-Schlüter current contours at two toroidal locations where the 16 3-axis magnetic coils were located.

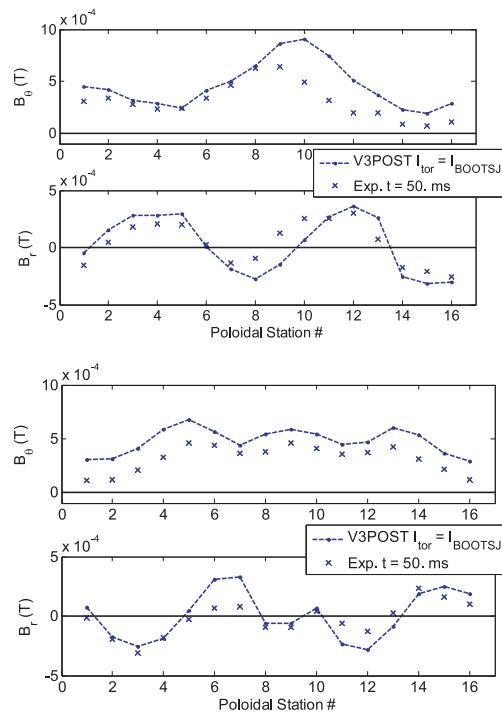


Fig. 5 Amplitude of magnetic field components (marked by “x”) in the poloidal and radial directions at the 1/6 field period (top) and 1/2 field period (bottom) locations. Also shown are the calculated values using the V3FIT code (dashed line).

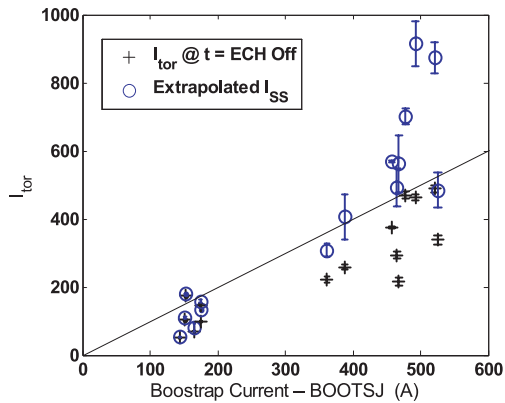


Fig. 6 Bootstrap current calculated by the BOOTSJ code compared with the measured current at the ECH turnoff (+) as well as an extrapolated value (\circ) of the current based on its time evolution.

Another interesting feature of Fig. 5 is that the poloidal magnetic field is offset vertically indicating that there is a current flowing in the plasma in addition to the Pfirsch-Schlüter current. We have made estimates of the bootstrap current in HSX using the BOOTSJ code [13] using the data from the Thomson scattering array as input. However, since the magnetic diffusion time is generally greater than the ECH pulse length, the total current measured by the Rogowski coil has not reached a steady-state by the end of the discharge.

A comparison of the current calculated by BOOTSJ with the measured current when the ECH turns off as well as an extrapolated steady-state value of the total current is shown in Fig. 6. The agreement is fairly good. In addition, the direction of the measured current is opposite from what it would be in a tokamak, as expected.

To model the signals detected by the 16 coil array, we use the V3FIT [14] code which takes as input the pressure and current profiles. When we include the current profile due to the bootstrap current in the V3FIT calculation, we obtain reasonably good agreement with the data that explains the vertical offset in the poloidal magnetic field. The calculation however does not take into account the evolution of the bootstrap current which could alter the agreement between the V3FIT code and the data. This will be addressed in the future. More information is provided in the paper by Schmitt [15].

4. Magnetic Flexibility

One of the best ways to test quasisymmetry is to degrade the symmetry and see what the result is on the plasma. To accomplish this, HSX has a set of 48 auxiliary planar coils that are outside the modular coil set that produces the quasihelical field. Depending on the arrangement of the coil distribution in the auxiliary coils, it is possible to vary the magnetic field spectrum as well as the rotational transform, well depth, neoclassical transport, par-

allel viscous damping and MHD stability.

In particular, one configuration is termed ‘Mirror’ because it introduces spectral terms with $(n, m) = (4, 0)$ and $(8, 0)$. The effect of these extra spectral terms is to increase the effective ripple at $r/a \sim 2/3$ from 0.005 to 0.04. The increase in the effective ripple is even larger towards the plasma core. For this configuration, the plasma volume, rotational transform, magnetic axis and well depth vary little from the QHS configuration. There is another, earlier, configuration called the ‘old Mirror’, which differs slightly from the ‘Mirror’ in the current distribution of the auxiliary coils. The ‘old Mirror’ had about a 1 cm magnetic axis shift between the QHS and ‘old Mirror’ that made it difficult to obtain a Thomson scattering profile that included the plasma core. For the ‘Mirror’ the shift is only about 1 mm. At first we will describe experiments that were done at a magnetic field of 0.5 T; further in the article we will discuss the 1.0 T data.

5. Trapped Particle Confinement

In the QHS configuration, calculations indicate that trapped particles should be very well confined. Similar calculations for the Mirror configurations show that the trapped particle confinement should be considerably degraded. We tested the trapped particle confinement by mounting a collector disk inside the vacuum chamber at the top and bottom of the confinement region and monitoring the floating potential [16].

Figure 7 shows the floating potential versus plasma density for the QHS and ‘old Mirror’ configurations. With quasisymmetry, the floating potential of the plates in both the ion and electron drift directions show little change as the density is varied. However, with the quasisymmetry degraded, the floating potential becomes increasingly negative at lower density. This is only observed in the direction of the electron drift, as expected. For the plate in the ion drift direction, the floating potential is relatively unchanged.

Another indication of the improved confinement of trapped particles with quasisymmetry is the higher x-ray flux in this configuration [17]. The hard x-ray emission in HSX was analyzed using a CdZnTe detector that was housed outside the vacuum vessel in a lead box with a 0.8 mm pinhole and a 200 mm SS filter. Pulse height analysis was used to obtain the energy spectrum in a set of similar ECH discharges. Figure 8 shows the spectrum for QHS and ‘old Mirror’ at the same density of $2 \times 10^{11} \text{ cm}^{-3}$. The high-energy tail for the QHS configuration is indicative of the improved confinement of the superthermal electrons that gives rise to the more efficient heating during the ECH.

6. Fluctuations at $B = 0.5 \text{ T}$

One distinguishing feature of the QHS configuration is the presence of a global coherent low-frequency mode that is observable from Langmuir probes, the interferome-

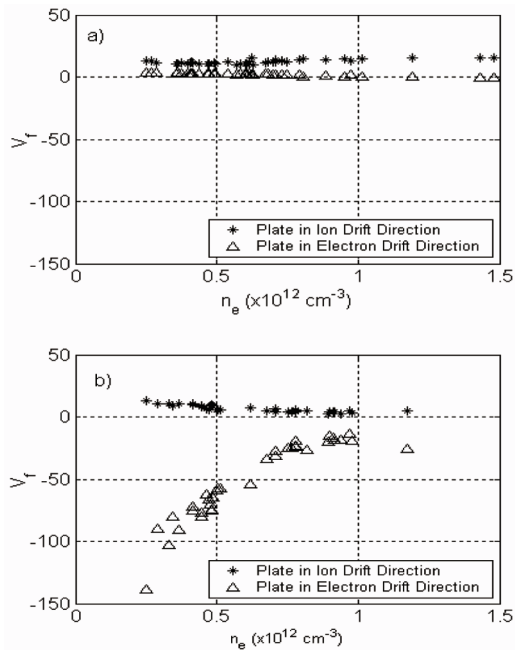


Fig. 7 Floating potential versus plasma density for the QHS configuration (top) and “old Mirror” configuration (bottom). Shown are the data for the plate in the ion (+) and electron (Δ) drift directions.

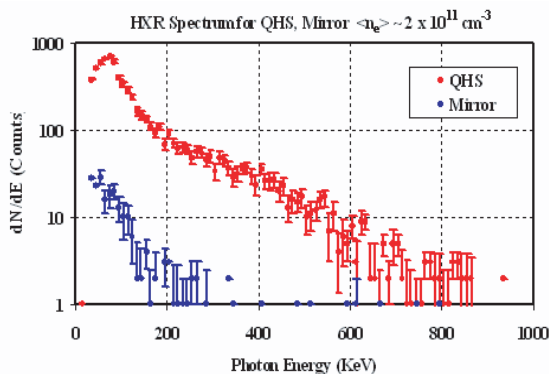


Fig. 8 X-ray spectrum for QHS and “old Mirror” configuration.

ter, the ECE radiometer as well as magnetic pick-up coils [18]. Indications from the interferometer, and more recently from a reflectometer, are that the mode is localized towards the plasma core. The estimated mode number is $n = 1$, $m = 1$. From probe measurements, the mode propagates in the electron diamagnetic direction. The mode frequency decreases with increasing density, in approximate agreement with an Alfvén mode. However, without a direct measurement of the electric field, it is difficult to determine the scaling in the laboratory frame of reference.

The striking feature of the mode is that it decreases in amplitude with increasing quasisymmetry degradation. Figure 9 shows a comparison of the frequency spectrum of density fluctuations measured by the reflectometer for the

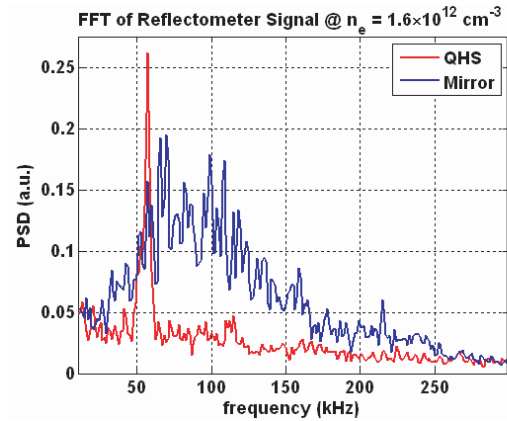


Fig. 9 Frequency spectrum of reflectometer signal for QHS and Mirror configurations at $r/a \sim 0.4$.

QHS and Mirror configurations [19]. The frequency of the reflectometer was tuned in this case to a spatial location of $r/a \sim 0.4$. In contrast to the broad turbulent spectrum for the Mirror configuration, the QHS spectrum is more quiescent, but with a large coherent mode at around 55 kHz. This mode is absent in the Mirror spectrum. Based on the measurements of an energetic tail population that is better confined in the QHS configuration, as discussed in the previous section, we infer that the coherent mode is most likely driven by nonthermal electrons. Future work will concentrate on whether the broader turbulent spectrum in the Mirror configuration might be due to the larger fraction of trapped particles for that configuration, close to the core.

7. Particle, Momentum and Heat Transport at $B = 0.5 \text{ T}$

A number of experiments were performed to compare particle, momentum and heat transport between the QHS and the Mirror configurations. More details are given in the papers by Gerhardt [20] and Canik [21]. A common feature of the experiments is that a reduction in neoclassical transport could be observed by altering the magnetic field spectrum, in approximate agreement with theory, but in each case there remained a large level of anomalous transport that didn't appear to change between the configurations.

Figure 10 shows the density profiles measured with a 10 channel Thomson scattering system. For the Mirror configuration, the profile is flat to hollow, which is typical of ECH discharges in many other stellarators. For the QHS configuration however, the profile is peaked. The experimental particle flux was inferred from a set of H_α detectors and the DEGAS [22] code. Inside $r/a \sim 0.3$, the experimental particle flux in the Mirror was found to be close to the neoclassical flux driven by temperature gradients. This flux, termed the thermodiffusive flux, is reduced in the QHS configuration, accounting for the peaked density

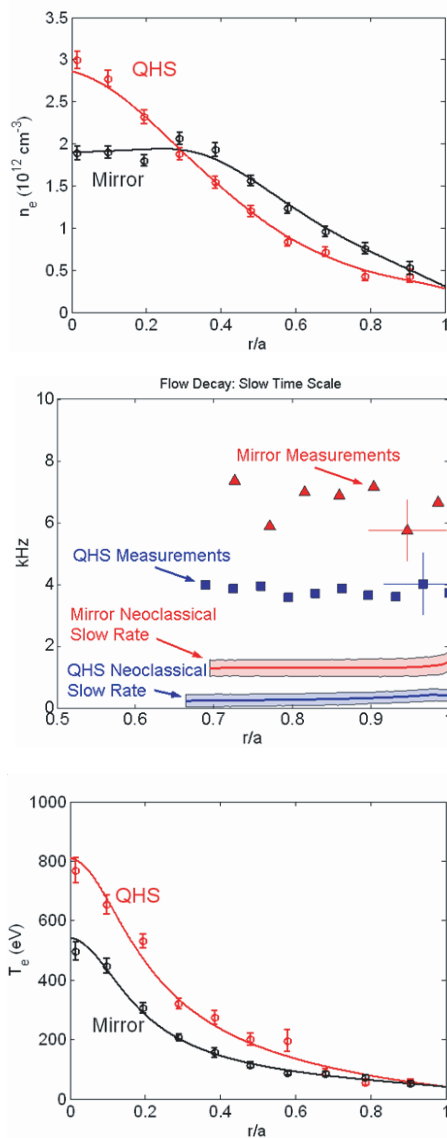


Fig. 10 Comparison of the density profile (top), flow decay rate (middle) and electron temperature profile (bottom) for QHS and Mirror configurations.

profile. In the outer regions of the plasma the experimental particle flux was found to be similar for the two configurations and, in both cases, much greater than the neoclassical level.

The middle figure of Fig. 10 shows the results of a comparative experiment using a biased electrode to spin up the plasma in the two configurations. It was found that for the quasisymmetric configuration, the plasma flow, as measured by a Mach probe, increased more slowly and rose to a higher value than for the Mirror configuration. After the bias turn-off, the decay in the flow was faster for the non-symmetric configuration. The results were compared to a neoclassical model which included damping due to parallel viscosity and neutral friction [23]. Solving two coupled momentum balance equations on a flux surface, the model calculates two time scales for the plasma flow, a

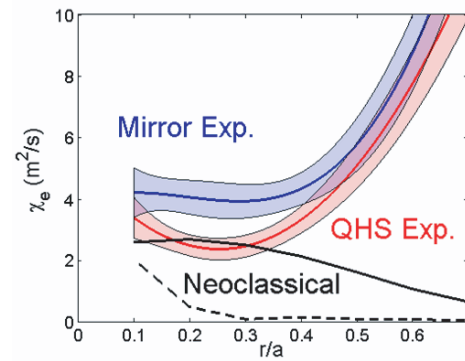


Fig. 11 Experimental and neoclassical thermal conductivities for the QHS and Mirror configurations.

faster and a slower time scale. The difference in the measured damping rates between the two magnetic configurations was roughly the same as the difference in the slow neoclassical rates. However, for both configurations, there is an additional source of flow damping that is unaccounted for in the neoclassical model.

The final comparison to be made is of the electron thermal diffusivity. The bottom plot of Fig. 10 shows the electron temperature profile for the two configurations with the same ECH input power. The central temperature is about 800 eV for the QHS configuration and 500 eV for the Mirror. The higher temperature for the quasisymmetric configuration is indicative of a lower neoclassical thermal conductivity.

A more rigorous comparison was made of the two configurations with the same temperature profile and similar density profiles, except for the core where thermodiffusion dominates for the Mirror. A comparison of the thermal conductivity for the two configurations is shown in Fig. 11. At $r/a \sim 0.2 - 0.3$, the electron thermal conductivity is around $2 \text{ m}^2/\text{s}$ for QHS and around $4 \text{ m}^2/\text{s}$ for Mirror. This difference is comparable to the difference in the neoclassical values. Towards the edge, where the neoclassical thermal conductivity is small, the two configurations have comparable transport.

8. Electron Thermal Conductivity at $B = 1.0 \text{ T}$

For second harmonic extraordinary mode heating at 0.5 T, the transport analysis was complicated by the presence of a superthermal electron population. This prevented an estimate of the absorbed power from being obtained based on the decay of the diamagnetic loop. Rather, a fairly tedious process of estimating the absorbed power was employed based on the time evolution of the total integrated kinetic energy obtained from Thomson scattering measurements. For fundamental ordinary mode heating at 1.0 T however, the superthermal population was much reduced based on diamagnetic, ECE and x-ray measurements. This

simplified the measurement of the absorbed power and the calculation of the thermal conductivity. Figure 12 shows that for 100 kW input power, electron temperatures up to 2.5 keV were obtained for the QHS configuration, while around 1.5 keV was measured for the Mirror.

The neoclassical and anomalous components of the total electron thermal conductivity were compared by matching as close as possible the temperature and density profiles. This required decreasing the QHS input power to 44 kW, while the Mirror input power stayed at 100 kW as in Fig. 12. The experimental and neoclassical electron thermal conductivities for the QHS and Mirror configurations are shown in Fig. 13. Still, roughly a factor of 3 reduction in the conductivity is observed at the plasma core due to the quasisymmetry. Further analysis is needed however at this point to understand how the anomalous transport compares between the two configurations. More details are given in the paper by Lore [24].

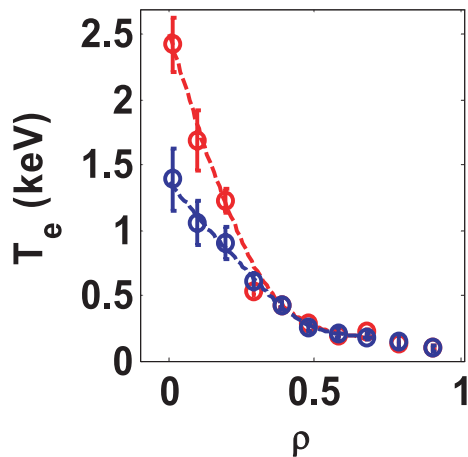


Fig. 12 Electron temperature profile for QHS (red) and Mirror (blue) with 100 kW input power. The parameter $\rho = r/a$ as in previous plots.

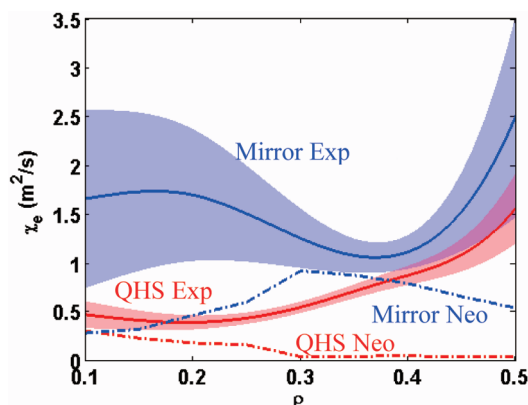


Fig. 13 Experimental and neoclassical electron thermal conductivities for QHS and Mirror.

9. Modeling Anomalous Transport in HSX

With ECH, the electron temperature in HSX is much higher than the ion temperature so that the dominant long wavelength instability is the trapped electron mode (TEM). Because of the quasisymmetry, the magnetic geometry in HSX looks similar to that in a tokamak with a high effective transform. In a comparison of microinstabilities in different stellarator geometries, Rewoldt [25] found that such modes in HSX had a fairly high growth rate because of this short connection length and also because of the substantial bad curvature at the location of the trapped particles.

To simulate anomalous transport in HSX, the Weiland ITG/TEM model [26], originally used to describe transport in tokamaks, was modified to approximate the local geometry in HSX. This required the substitution of the helical ripple in place of the toroidal ripple and a local curvature about 3 times that of a tokamak with the same major radius. The 3D gyrokinetic code GS2 [27] was then used to confirm that the linear growth rates using the modified Weiland model were accurate to within 30%. Details are given in the paper by Guttenfelder [28].

The temperature profile in HSX was modeled by assuming a thermal conductivity consisting of the neoclassical term and the Weiland contribution. The power deposition profile is based on a calculation using a ray-tracing code and the total absorbed power comes from the decay of the diamagnetic loop signal. Figure 14 shows a comparison of the experimental data to the model calculation. Outside the region of $r/a \sim 0.3$, the agreement is quite good. Towards the core the agreement isn't as good, possibly because of the omission of non-linear effects or $E \times B$ shear suppression of turbulence. The predicted energy confinement times agree well with the experimental confinement times. The dependence of the experimental confinement time on the absorbed power is slightly weaker than the model prediction. This is shown in Fig. 15.

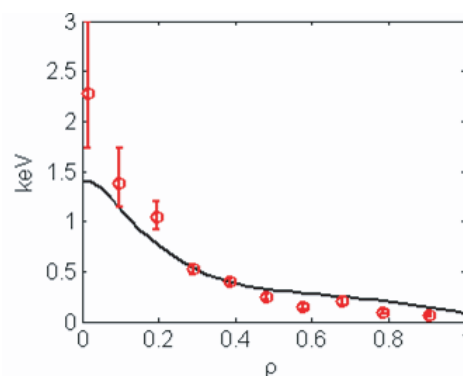


Fig. 14 Electron temperature profile from Thomson scattering (red circles) and model (black line).

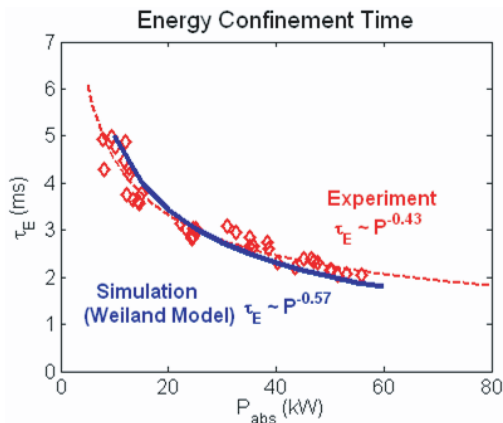


Fig. 15 Comparison of model dependence of confinement time (blue line) on absorbed power with experimental data (red diamonds).

10. Conclusions

This paper reviewed a number of different ways in which quasisymmetry was tested in HSX. A quasihelically symmetric configuration is noted for its lack of toroidal curvature and high effective transform. The high effective transform was confirmed by observing the small deviation of a passing particle orbit from a magnetic surface and by measuring the relatively small PS and bootstrap currents. The lack of toroidal curvature was noted by the drift of an electron to the inside of the flux surface, rather than to the outside if toroidal curvature dominated. Also, the helical PS current and the direction of the bootstrap current were also indications of a very small toroidal curvature. Measurements of the poloidal and radial components of the magnetic field due to the plasma currents showed good agreement with the V3FIT code.

Another feature of the quasisymmetric configuration is the good confinement of energetic trapped particles as seen from collector plates and hard x-ray measurements. This good confinement may be responsible for an MHD instability which is observed to decrease in amplitude and then disappear as the degree of quasisymmetry breaking increases. First measurements of density fluctuations at the plasma core were obtained with a reflectometer and showed a quiescent background plasma with a large coherent global mode for the QHS configuration, versus a broad spectrum of turbulent fluctuations without the coherent mode for the Mirror configuration.

With ECH at a magnetic field of 0.5 T, the results showed that the parallel momentum damping, particle thermodiffusion and electron thermal conductivity could all be decreased with quasisymmetry. The level of decrease roughly agreed with the calculated decrease in the neoclassical values, however a large anomalous component to particle, momentum and heat transport still remained. To date, there is no evidence in the data obtained at 0.5 T that the anomalous contribution differs substantially between the quasisymmetric and nonsymmetric configurations.

At a magnetic field of 1.0 T, central electron temperatures were up to 2.5 keV for the QHS configuration when 100 kW ECH was injected into the plasma. With the quasisymmetry degraded, the core temperature fell to 1.5 keV. Analysis of the transport for similar temperature and density profiles showed substantial reduction in the experimental thermal conductivity at the plasma core with quasisymmetry. Further analysis is needed before it can be understood whether the anomalous transport for the QHS case was different from that in the Mirror configuration.

Finally, while the short connection lengths in HSX were shown to be good for decreasing particle orbit deviations from a flux surface as well as lowering plasma currents and neoclassical transport, initial evidence seems to indicate that the combination of the short connection lengths and large curvature may be responsible for somewhat higher anomalous transport. Calculations of the temperature profile and energy confinement time based on a combination of neoclassical transport plus a modified Weiland model for anomalous transport, show reasonable agreement with the data. So far the model ignores zonal flows, $\mathbf{E} \times \mathbf{B}$ shear suppression of turbulence, nonlinear effects and the differences in the fraction of trapped particles between the quasisymmetric and nonsymmetric configurations. Future work will concentrate on understanding how the degree of quasisymmetry affects the radial electric field and plasma turbulence.

In summary then, initial experimental results indicate that the quasisymmetric configuration has fulfilled its promise of reducing neoclassical transport. More work is needed to resolve what effect the quasisymmetric configuration has on anomalous transport.

Acknowledgments

The authors wish to thank the V3FIT team for the use of their code and especially Steve Knowlton for invaluable assistance. This work was supported by the U.S. Department of Energy under Contract No. DE-FG02-93ER54222.

- [1] H.E. Mynick, *Phys. Plasmas* **13**, 058102 (2006).
- [2] J. Nührenberg and R. Zille, *Phys. Lett. A* **129**, 113 (1988).
- [3] P.R. Garabedian, *Phys. Plasmas* **4**, 1617 (1997).
- [4] H. Sugama and T.-H. Watanabe, *Phys. Rev. Lett.* **94**, 115001 (2005).
- [5] H.E. Mynick and A.H. Boozer, *Phys. Plasmas* **14**, 072507 (2007).
- [6] F.S.B. Anderson *et al.*, *Fusion Technol.* **27**, 273 (1995).
- [7] G.H. Neilson, M.C. Zarnstorff, J.F. Lyon and the NCSX Team, *J. Plasma Fusion Res.* **78**, 214 (2002).
- [8] D.A. Spong, S.P. Hirshman, L.A. Berry *et al.*, *Nucl. Fusion* **41**, 711 (2001).
- [9] J.N. Talmadge, V. Sakaguchi, F.S.B. Anderson, D.T. Anderson and A.F. Almagri, *Phys. Plasmas* **8**, 5165 (2001).
- [10] A.H. Boozer, *Phys. Fluids* **24**, 1999 (1981).
- [11] A.H. Boozer and H.J. Gardner, *Phys. Fluids B* **2**, 2408 (1990).

- [12] K.C. Shaing and J.D. Callen, *Phys. Fluids* **26**, 3315 (1983).
- [13] K.C. Shaing *et al.*, *Phys. Fluids B* **4**, 148 (1989).
- [14] S.P. Hirshman, E.A. Lazarus, J.D. Hanson, S.F. Knowlton and L.L. Lao, *Phys. Plasmas* **11**, 595 (2004).
- [15] J.C. Schmitt, J.N. Talmadge, P.H. Probert and D.T. Anderson, *Proceedings of ITC/ISHW2007*.
- [16] J.M. Canik, *Bull. Am. Phys. Soc.* **47**, 76 (2002).
- [17] A. Abdou, Ph. D. thesis, University of Wisconsin-Madison (2005).
- [18] D.L. Brower, C. Deng *et al.*, *Transport Task Force, 2005*.
- [19] K. Likin *et al.*, *Proceedings of ITC/ISHW2007*.
- [20] S.P. Gerhardt, J.N. Talmadge, D.T. Anderson and J.M. Canik, *Phys. Plasmas* **12**, 56116 (2005).
- [21] J.M. Canik, D.T. Anderson, F.S.B. Anderson, C. Clark, K.M. Likin, J.N. Talmadge and K. Zhai, *Phys. Plasmas* **14**, 056107 (2007).
- [22] D. Heifetz *et al.*, *J. Comput. Phys.* **46**, 309 (1982).
- [23] M. Coronado and J.N. Talmadge, *Phys. Fluids B* **5**, 1200 (1993).
- [24] J. Lore *et al.*, *Proceedings of ITC/ISHW2007*.
- [25] G. Rewoldt, L.-P. Ku and W.M. Tang, *Phys. Plasmas* **12**, 102512 (2005).
- [26] H. Nordman *et al.*, *Nucl. Fusion* **30**, 983 (1990).
- [27] M. Kotschenreuther *et al.*, *Comp. Phys. Comm.* **88**, 128 (1995).
- [28] W. Guttenfelder *et al.*, *Proceedings of ITC/ISHW2007*.